International Journal of Mass Spectrometry 304 (2011) 45–50

Contents lists available at ScienceDirect

International Journal of Mass Spectrometry

journal homepage: www.elsevier.com/locate/ijms

Dissociative photoionization of $CH_3C(O)CH_2$ to $C_2H_5^+$

Bridget W. Alligood, Caroline C. Womack, Matthew D. Brynteson, Laurie J. Butler*

The James Franck Institute and Department of Chemistry, University of Chicago, Chicago, IL 60637, USA

ARTICLE INFO

Article history:
Received 18 January 2011
Received in revised form 29 March 2011
Accepted 30 March 2011
Available online 8 April 2011

Keywords:
Dissociative photoionization
$CH_3C(O)CH_2$ radical
Daughter fragmentation
Crossed laser-molecular beam scattering
Velocity map imaging

ABSTRACT

We use a combination of crossed laser-molecular beam scattering experiments and velocity map imaging experiments to investigate the dissociative ionization of the $CH_3C(O)CH_2$ radical to $C_2H_5^+$. We form the radical from C–Cl bond fission in the photodissociation of chloroacetone at 193 nm. Upon 10.5 eV VUV photoionization, the radical is not detected at a parent mass-to-charge ratio of 57, but instead is only detected at the fragment $m/z = 29$ ($C_2H_5^+$). While the appearance of multiple daughter ions is expected, and indeed observed, using 200 eV electron bombardment ionization, one normally expects "soft" VUV photoionization to give signal at parent ion. We present electronic structure calculations that offer an explanation of our experimental results. The results presented herein also confirm the presence of a minor dissociation channel for the highly vibrationally excited $CH_3C(O)CH_2$ radicals – one that forms $C_2H_5 + CO$ following isomerization to CH_3CH_2CO.

1. Introduction

Both electron bombardment ionization and vacuum-ultraviolet (VUV) photoionization are common ionization methods employed in the detection schemes for both molecules and radicals. The choice of method often depends on the type of experiment, as there are advantages and disadvantages inherent to both. Electron bombardment ionization, specifically at high energies, is very general; it is typically thought of as a universal method, but it often results in a great deal of dissociative ionization of parent species. Lower energy ionization methods, whether low-energy electron bombardment ionization [1] or VUV photoionization [2], are typically referred to as "soft" ionization methods, as they usually result in little or no dissociative ionization. The merits and successes of these "soft" ionization techniques, for radicals in particular, have been demonstrated thoroughly [3–5].

We recently investigated [6] the primary photodissociation channels of chloroacetone at 193 nm. Our data revealed that there were two major primary channels, C–Cl fission producing Cl and $CH_3C(O)CH_2$, as well as C–C fission to produce CH_3CO and CH_2Cl. We have since taken data to characterize a third photodissociation channel, one that yields CH_3 and $COCH_2Cl$ [7]. We used the crossed laser-molecular beam scattering apparatus to measure the distribution of velocities imparted to the Cl atoms upon C–Cl bond fission; the momentum-matched $CH_3C(O)CH_2$ radicals were formed under collision-free conditions, which facilitated characterization of their internal energy distribution and subsequent dynamics. Our results showed that some of the nascent $CH_3C(O)CH_2$ radicals were formed with a low enough internal energies to be stable to dissociation. Using a combination of the crossed laser-molecular beam scattering measurements and velocity map imaging, we were then able to detect and characterize the dissociation products of the higher internal energy radicals. In the process, we noted the absence of $m/z = 57$ ($CH_3C(O)CH_2^+$) parent ions from both 200 eV electron bombardment ionization and 10.5 eV photoionization. While our data revealed that stable neutral radicals were indeed present, they interestingly were not detected at their parent mass-to-charge ratio in either experiment. Although this is far from surprising using 200 eV electron bombardment ionization, the "softer" photoionization methods are typically employed in attempts to reduce dissociative ionization. There are, however, a few cases in which even the "softest" of ionization methods results in fragmentation. As an example, experimental studies [8,9] have detected not CH_3O^+, but rather CHO^+ upon electron-bombardment ionization and photoionization of the CH_3O radical. Theoretical work by Harvey and Aschi showed that the CH_3O^+ cation dissociates to $CHO^+ + H_2$ via intersystem crossing from the triplet state of the CH_3O^+ cation to a repulsive singlet state that correlates to $CHO^+ + H_2$ [10], even when the cation is formed in the zero-point vibrational state. The results presented in this paper proceed through a different mechanism for efficient dissociative ionization. In this case, there is no local minimum at a $CH_3C(O)CH_2^+$ isomer on the cation's potential energy surface; upon vertical excitation, the cation first isomerizes and then dissociates. Thus, this species cannot be detected at parent ion, even at a 10.5 eV photoionization energy; instead, it is detected at the $C_2H_5^+$ product mass-to-charge ratio. We present both computational and experimental results that support this mechanism for the case of the $CH_3C(O)CH_2$ radical.

* Corresponding author. Tel.: +1 773 702 7206.
E-mail address: L-Butler@uchicago.edu (L.J. Butler).

1387-3806/$ – see front matter © 2011 Elsevier B.V. All rights reserved.
doi:10.1016/j.ijms.2011.03.012

While many species isomerize when photoionized [11,12], such as the ethyl cation [12] whose minimum structure is a bridged one, they can still be detected at parent ion. Others exhibit dissociative ionization when there is a local minimum near the vertical geometry, but the internal energy of the cation is sufficiently high to allow isomerization on the cationic surface and subsequent dissociation (see Refs. [13–15] for a few examples). Dissociative ionization at very low photoionization energies, as investigated here, is much less common.

2. Methods

For ease of communication, all energetic values given in this paper are presented in units of electron volts (eV); the conversion to the SI unit for energy (Joule) is 1 eV = 1.602×10^{-19} J.

Two complementary experimental techniques are described in the following sections. The primary difference in these two techniques, as least as highlighted in this paper, is regarding the method of ionization; the crossed laser-molecular beam scattering apparatus employs 200 eV electron bombardment ionization, while the velocity map imaging apparatus uses 10.5 eV photoionization.

2.1. Experimental method – imaging apparatus

The velocity map imaging (VMI) apparatus used in this work has been described previously [16–20]; the relevant experimental conditions have also been detailed in our previous work on this system [6]. Briefly, we expand the molecular beam, composed of the vapor pressure of chloroacetone seeded in He to a total backing pressure of 400 Torr, through a pulsed valve; we heat the nozzle, which has a 0.8 mm diameter, to 80 °C. After passing through a skimmer, the molecules are photodissociated with a vertically polarized 193.3 nm beam.

The photofragments are ionized by 118 nm (10.5 eV) light, delayed ~40 ns after the photodissociation laser [20]. The $CH_3C(O)CH_2$ neutral photofragment is imparted a velocity in the photodissociation. If the cation also dissociates, an additional velocity is imparted to the products from this dissociative photoionization. The recoiling ions form a spherically expanding cloud, which travels down a grounded time-of-flight tube toward the detector. The detector consists of a position-sensitive microchannel plate assembly (MCP) coupled to a phosphor screen. We pulse the voltage on the front plate of the MCP to −750 V in order to coincide with the arrival time of ions having the desired mass-to-charge ratio. A cooled charge-coupled device (CCD) camera records images of the ions. We process the obtained images using the ion-counting method, and the raw images are symmetrized about the vertical and horizontal axes in the data analysis.

2.2. Experimental method – scattering apparatus

We also use a crossed laser-molecular beam scattering apparatus to measure the photofragment velocities resulting from C–Cl bond fission in the photodissociation of chloroacetone, $CH_3C(O)CH_2Cl$. The experimental details relevant to this system, both experimental conditions and defined apparatus parameters, have been described previously [6]. Briefly, we expand the molecular beam, composed of chloroacetone seeded in He to a total stagnation pressure of 400 Torr, through a continuous (not pulsed) nozzle. The nozzle has a 0.15 mm diameter, and we heat it to 180 °C. The molecular beam source can be rotated to different angles in the plane containing the beam and the detector axis; for the spectrum shown in this paper the data were acquired with a source angle of 10°. The molecular beam passes through two skimmers before it enters the main chamber, where it intersects the output of a 193.3 nm excimer laser. The neutral photodissociation products scatter from the interaction region with velocities determined by the vector sum of the molecular beam velocity and the recoil velocity imparted during the photodissociation. Those fragments that scatter into the detector are ionized by 200 eV electrons [21]. High voltage lenses accelerate and focus these ions toward the entrance of a quadrupole mass spectrometer, where they are mass-selected and detected using a Daly detector [22]. The signal is recorded as a function of time after the dissociating light pulse. Upon subtraction of the calibrated ion flight time, forward convolution fitting of the time-of-flight (TOF) spectrum determines the distribution of energies imparted to relative product translation during the dissociation, E_T.

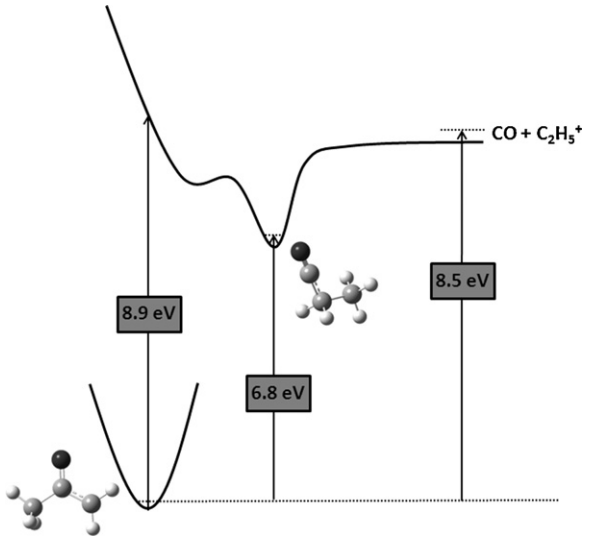

Fig. 1. The energies for the relevant minima and transition states of the $CH_3COCH_2^+$ cation potential energy surface. All points are calculated at the G3//B3LYP level of theory. The structures were optimized at the B3LYP level of theory, using an aug-cc-pVTZ basis set, and they were converged to a root-mean-square (RMS) force below 1×10^{-5} and a RMS displacement below 4×10^{-5}, both in atomic units. All energies except the vertical ionization energy are zero point corrected; they are presented relative to the neutral $CH_3C(O)CH_2$ radical, as indicated by the arrows.

2.3. Computational methods

The minima and transition states relevant to the dissociative ionization of the $CH_3C(O)CH_2$ radical are calculated with the modified G3//B3LYP method [23] using the GAUSSIAN03 electronic structure package [24]. We optimize the geometries of each minimum and transition state, calculated using the B3LYP method with a aug-cc-pVTZ basis set and a spin-unrestricted reference. The geometries are converged to a root-mean-square (RMS) force below 1×10^{-5} and a RMS displacement below 4×10^{-5}, where both are in atomic units.

3. Results and analysis

3.1. Computational results on the cationic surface of $CH_3C(O)CH_2$

To begin our work on this system, we calculated the vertical and adiabatic ionization energies for the $CH_3C(O)CH_2$ radical formed from 193 nm photodissociation of chloroacetone. Our results, calculated at the G3//B3LYP/aug-cc-pVTZ level of theory, are shown in Fig. 1. They reveal that the $CH_3C(O)CH_2^+$ cation can undergo a nearly barrierless isomerization to $CH_3CH_2CO^+$; accordingly, we were unable to identify a transition state between the two structures. The $CH_3CH_2CO^+$ ion can then dissociate to $CO + C_2H_5^+$ via a loose transition state with no barrier beyond the endoergicity. Both the iso-

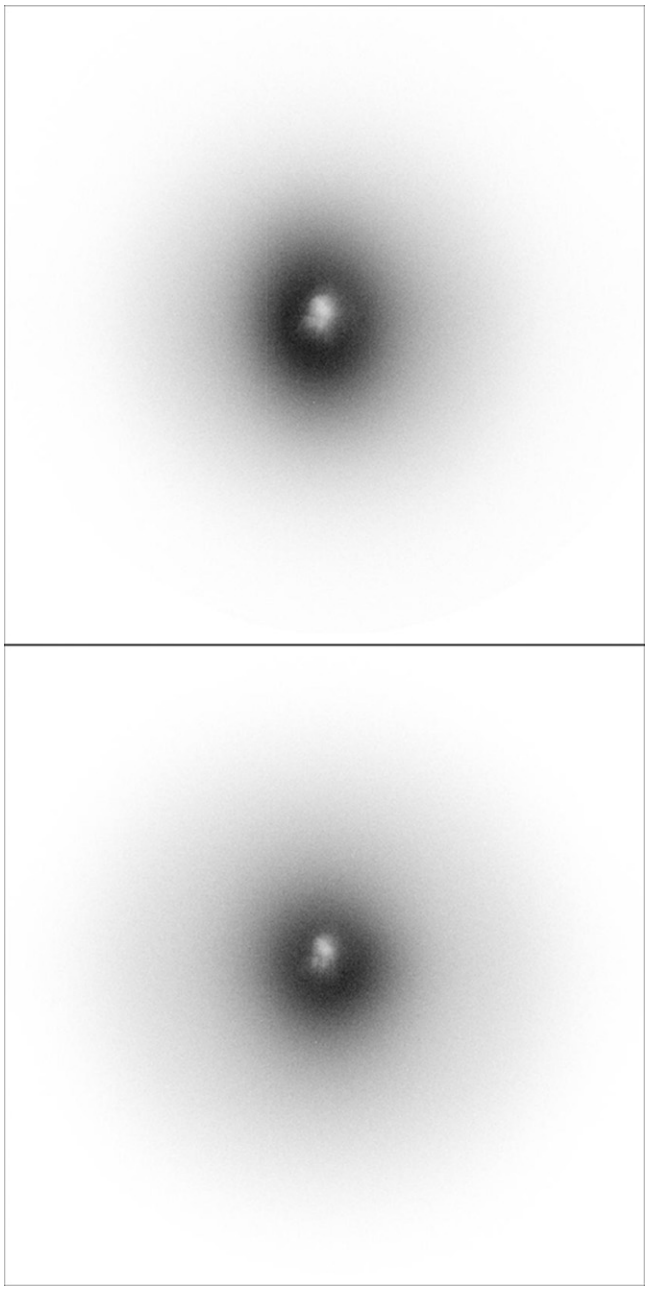

Fig. 2. Raw images of the $m/z = 29$ ($C_2H_5^+$) and $m/z = 27$ ($C_2H_3^+$) products, shown in the upper and lower frames, respectively. Both were obtained with 118 nm photoionization following photodissociation of chloroacetone at 193 nm. The images are 841 × 841 pixels and are the result of subtracting the background images, obtained with 193 nm only and 118 nm only, from the raw data.

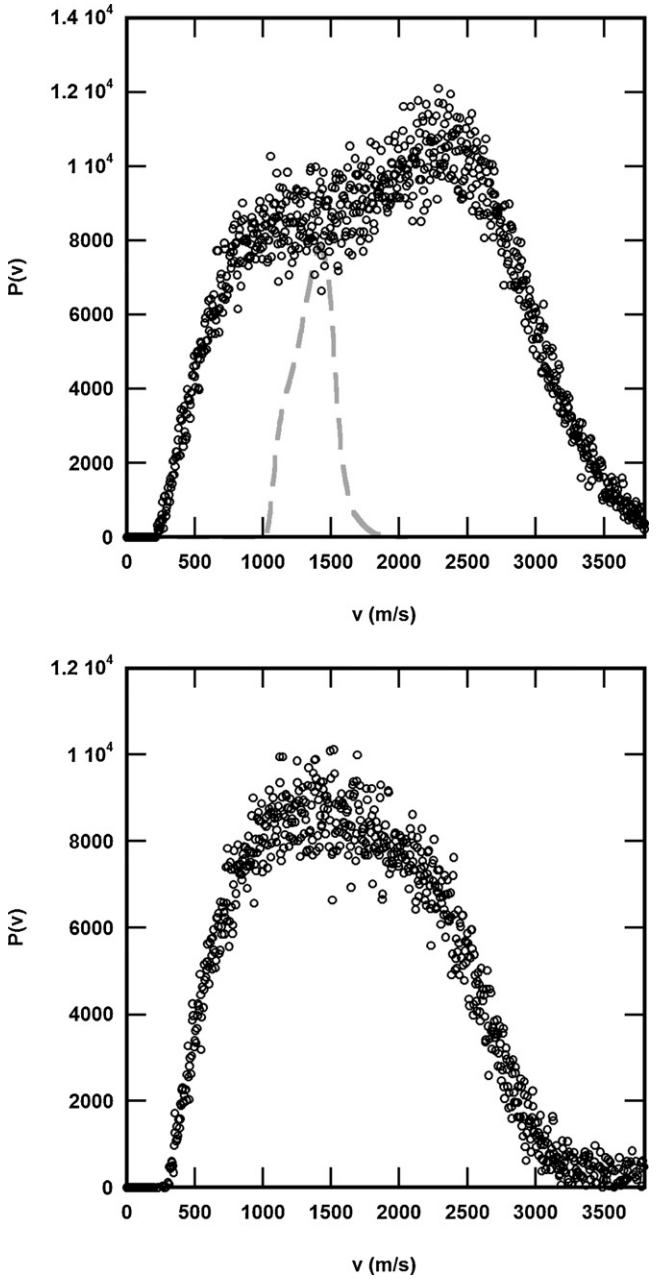

Fig. 3. Background-subtracted speed distributions of the $m/z = 29$ ($C_2H_5^+$) and $m/z = 27$ ($C_2H_3^+$) products from the imaging experiments, shown with open circles in the upper and lower frames, respectively. These speed distributions are derived from the images shown in Fig. 2. The fact that these distributions are identical at the slower speeds hints that the $m/z = 27$ signal is from the dissociative ionization of the neutral mass 29 (C_2H_5) products formed from the secondary dissociation of vibrationally excited $CH_3C(O)CH_2$ radicals. The dashed gray line in the upper frame shows a comparison to the measured speed distribution of stable $CH_3C(O)CH_2$ products (derived from the short-dashed line component of the C–Cl bond fission $P(E_T)$ shown in Fig. 5 of Ref. [6]). The $m/z = 29$ products have a broader distribution of speeds than the stable radicals from which they are formed; this reflects the extra recoil velocities that are imparted to the $C_2H_5^+$ ions as the $CH_3C(O)CH_2^+$ cation isomerizes and then dissociates to $C_2H_5^+ + CO$ (see Fig. 1).

merization and ultimate dissociation are well below the 10.5 eV of available energy, resulting in the stable $CH_3C(O)CH_2$ radicals being detected at $m/z = 29$ ($C_2H_5^+$) rather than at $m/z = 57$ ($CH_3C(O)CH_2^+$).

3.2. Imaging experiments

Fig. 2 shows images acquired at $m/z = 29$ ($C_2H_5^+$) and $m/z = 27$ ($C_2H_3^+$) in the upper and lower frames, respectively. The corresponding speed distributions are shown in Fig. 3. The $m/z = 27$ distribution spans speeds that are identical to the slower $m/z = 29$ signal; this implies that the $m/z = 27$ and a portion of the $m/z = 29$ signal are from the same neutral photofragment. Indeed, calculations by FitzPatrick reveal a minor isomerization channel of $CH_3C(O)CH_2$ radical (most dissociate to CH_3 + ketene) resulting in CH_3CH_2CO; the CH_3CH_2CO isomer can then dissociate to CH_3CH_2 (mass 29) + CO (mass 28) [25]. We assign all of the $m/z = 27$ signal to the dissociative ionization of this mass 29 fragment to $m/z = 27$; the calculated appearance energy of $C_2H_3^+$ from neutral C_2H_5 is 10.0 eV at the G3//B3LYP/aug-cc-pVTZ level of theory. The $m/z = 29$ signal evidences both the signal from C_2H_5 at parent ion from the

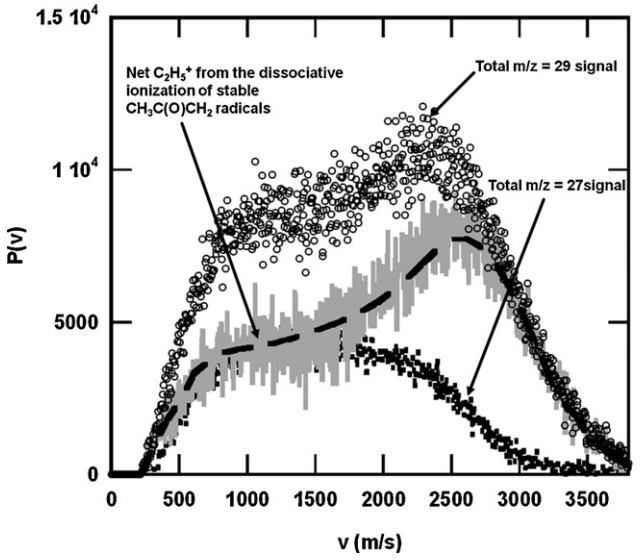

Fig. 4. Background-subtracted speed distributions of the $m/z = 29$ ($C_2H_5^+$) and $m/z = 27$ ($C_2H_3^+$) products from the imaging experiments, shown with open circles and dotted black line, respectively. The solid gray line shows the difference in signal between $m/z = 29$ and $m/z = 27$; this signal is attributed to $C_2H_5^+$ products from the dissociative ionization of stable mass 57. The remaining signal, appearing at both $m/z = 27$ and at $m/z = 29$, is from photoionization of the C_2H_5 products from a minor neutral photodissociation channel of the $CH_3C(O)CH_2$ radical (see text). The long-dashed black line is the fit obtained by explicitly considering the velocities imparted in the primary photodissociation, along with those imparted as the stable radicals dissociatively ionize to $C_2H_5^+ + CO$. The secondary $P(E_T)$ that gives this fit is shown in Fig. 5.

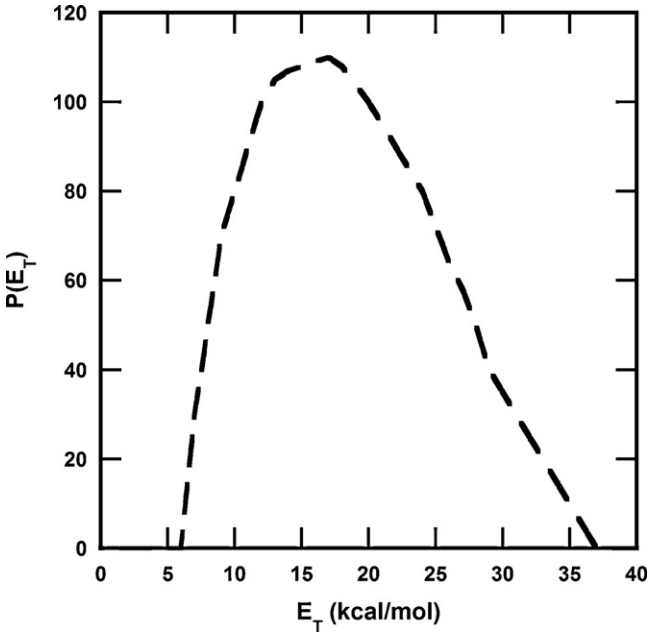

Fig. 5. The secondary recoil translational energy distribution, $P(E_T)$, for the dissociative ionization of stable $CH_3C(O)CH_2$ radicals to $C_2H_5^+ + CO$. Forward convolution fitting of the data shown in solid gray line in Fig. 4 was used to derive this $P(E_T)$. For the primary C–Cl bond fission, the higher kinetic energy portion of the overall $P(E_T)$ shown in Fig. 5 of Ref. [6] was considered; this portion is shown in short-dashed gray line in that figure. The $P(E_T)$ shown here is used to calculate the additional velocity imparted as the stable $CH_3C(O)CH_2$ radicals dissociatively ionize to $C_2H_5^+ + CO$.

aforementioned process and the signal from the dissociative ionization of the mass 57 ($CH_3C(O)CH_2$) parent radical. To get the "net" $m/z = 29$ signal, resulting from only the dissociative ionization of $CH_3C(O)CH_2$, we iteratively subtracted the $m/z = 27$ signal from the total $m/z = 29$ signal in order to achieve a distribution that we could fit using the two-step process described in the next paragraph.

The remaining $m/z = 29$ signal, that assigned to dissociative ionization of the $CH_3C(O)CH_2$ radical is shown in solid gray line in Fig. 4. Because the stable $CH_3C(O)CH_2$ neutral species are rotationally excited (see Ref. [6]), the rotational energy can be carried over to the cation upon photoionization; this results in additional recoil velocity imparted to the $C_2H_5^+$ ion and the neutral CO partner as the cation dissociates. To illustrate the additional velocity imparted in the dissociation, the upper frame of Fig. 3 shows a comparison of the measured speed distribution of the $C_2H_5^+$ ion with the speed distribution of the neutral stable radicals detected in our scattering experiments (see Ref. [6]); the dashed gray line in that frame then shows where the $C_2H_5^+$ signal would result, were there no additional velocity imparted upon secondary dissociation. To fit the observed signal, shown in solid gray line in Fig. 4, we modeled this dissociation using the range of recoil velocities imparted in the initial photodissociation of chloroacetone (see Ref. [6]) along with the range of recoil velocities imparted in the dissociation on the cationic surface. The fit from modeling this two-step process is shown by long-dashed black line in Fig. 4, and the secondary $P(E_T)$ used to obtain this fit is given in Fig. 5.

When fitting the data in Fig. 4, we had to specify the angular distribution of the velocity vector of the $C_2H_5^+$ and CO products with respect to the velocity of the cation that dissociated to give these products. Assuming that all azimuthal angles ϕ are equally likely, which is the case for any given velocity vector of the dissociating cation, the angular distribution can be determined by comparing the dissociation lifetime compared to the rotational period. If the dissociation lifetime is long with respect to the rotational period of the cation, the recoil direction of the products is uniformly distributed in the plane of rotation, θ. The angular distribution, therefore, is uniform in both θ and ϕ, leading to $I(\theta) = 1/\sin\theta$ in the expression $I(\theta)\sin\theta d\theta d\phi$; the z axis is defined as the direction of the velocity vector of the species that is undergoing secondary dissociation, the $CH_3C(O)CH_2^+$ cation, in the center-of-mass reference frame [26]. As this $I(\theta)$ increases dramatically at 0 and 180°, we leveled out the function at $\cos\theta = \pm 0.9875$. The resulting $I(\theta)$ angular distribution is shown in dashed black line in Fig. 6; it is symmetric and strongly forward–backward peaked, as expected for the

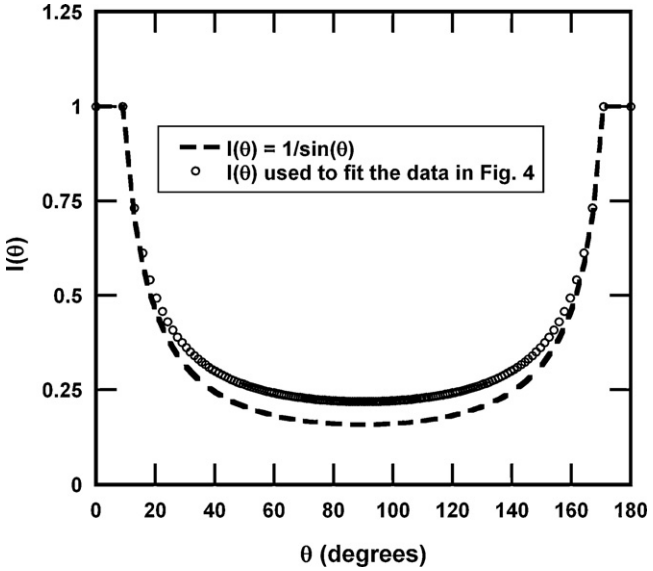

Fig. 6. Angular distribution assumed for the dissociation of $CH_3C(O)CH_2^+$ cations. The angle θ is the angle between the velocity vector (in the center-of-mass reference frame) of the cation that dissociates and the direction of recoil of the product from that dissociation. The angular distribution is generated by assuming that the dissociation lifetime of the cation is long with respect to its rotational period.

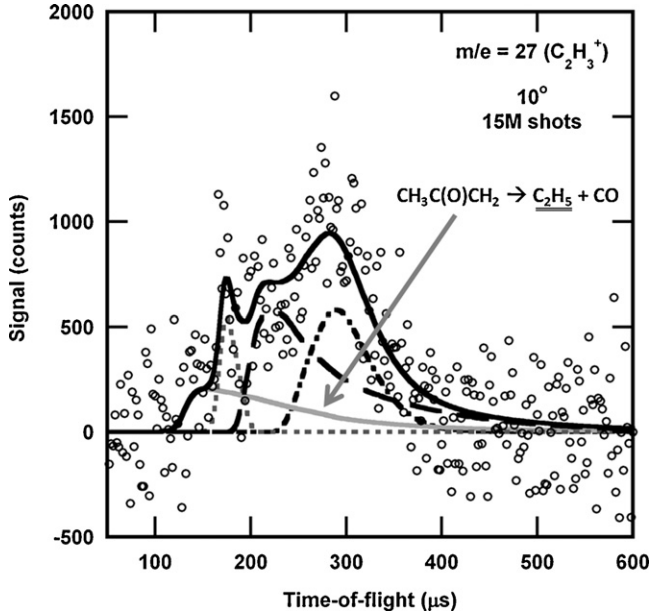

Fig. 7. Time-of-flight spectra of the signal at $m/z = 27$ ($C_2H_3^+$) resulting from the photodissociation of chloroacetone and the subsequent dissociation of $CH_3C(O)CH_2$ radicals formed upon C–Cl bond fission, as well as dissociative ionization of the CH_3CO products formed upon primary C–C bond fission. The data are shown in open circles, and the overall fit shown in solid black line. The spectrum contains contributions from neutral CH_3CO photoproducts dissociatively ionizing to $m/z = 27$, stable mass 57 $CH_3C(O)CH_2$ radicals dissociatively ionizing to $m/z = 27$, and dissociative ionization of molecular clusters $(CH_3C(O)CH_2)_n$ in the beam – all upon 200 eV electron bombardment ionization. These fits are shown in long-dashed black line, dotted gray line, and dash-dot-dashed black line, respectively and are described in detail in our previous publication [6]. The signal assigned to neutral C_2H_5 products, as predicted from the imaging $P(v)$ for the $m/z = 27$ signal, is shown in solid gray line.

highly rotationally excited $CH_3C(O)CH_2^+$ cation. We used a modified version of this $1/\sin\theta$ distribution to fit the data shown in Fig. 4; we justify this by the fact that the ions are experiencing repulsive forces as they dissociate, perhaps distorting the secondary angular distribution from the expected $1/\sin\theta$ distribution; the distribution that we actually used is shown in open circles in Fig. 6, and some of the relative intensity has been increased at around $\theta = 90^\circ$.

3.3. Scattering experiments

We also took data at $m/z = 29$ ($C_2H_5^+$) and $m/z = 27$ ($C_2H_3^+$) in the scattering lab. While little to no signal appeared above the noise in the $m/z = 29$ spectrum, the $m/z = 27$ spectrum revealed signal in good qualitative agreement with the imaging results. The spectrum, with its momentum-matched fit, is shown in Fig. 7. The components to this fit include the dissociative ionization of molecular clusters in the beam (shown in black dash-dot-dashed line), dissociative ionization of CH_3CO neutral photofragments following initial C–C bond fission in chloroacetone (shown in long-dashed black line), dissociative ionization of stable $CH_3C(O)CH_2$ radicals (shown in dashed gray line), and the time-of-flight predicted by the $m/z = 27$ imaging $P(v)$ and the slow component in the $m/z = 29$ $P(v)$. The first three of these contributors were described in detail in Ref. [6].

4. Discussion

This work investigated the photoionization of stable $CH_3C(O)CH_2$ radicals formed from the photodissociation of chloroacetone at 193 nm. We found that, even using 10.5 eV photons to photoionize these radicals, no signal was detected at parent ion ($m/z = 57$); instead, signal appeared at $m/z = 29$. The cation is thus dissociating to give $C_2H_5^+ + CO$.

The data presented in Ref. [6] showed that, while a large fraction of the $CH_3C(O)CH_2$ radicals formed in the photodissociation of chloroacetone at 193 nm are formed stable to secondary dissociation, these stable radicals are detected at multiple daughter ions upon 200 eV electron bombardment ionization; these daughter ions include $m/z = 15$ (CH_3^+) and $m/z = 42$ ($COCH_2^+$). This is not surprising, as 200 eV electron bombardment ionization often results in dissociative ionization. We sought to detect the same stable radicals at parent $m/z = 57$ ($CH_3C(O)CH_2^+$) by using 10.5 eV photoionization – a "softer" ionization method which tends to minimize such daughter fragmentation. Even with 10.5 eV photoionization, however, no parent signal was detected; instead, signal from the efficient dissociative ionization of this radical to $m/z = 29$ was observed. We investigated the cationic surface computationally, revealing a mechanism by which, even upon 10.5 eV photoionization, the parent $CH_3C(O)CH_2$ radical could dissociatively ionize to $C_2H_5^+ + CO$; this occurred via an isomerization and subsequent dissociation on the cationic surface. This mechanism is quite different from other situations where, at low enough energies, photoionization could result in detection at the parent mass-to-charge ratio [13–15]. In our case, there is no local minimum at the $CH_3C(O)CH_2^+$ cation's isomer, so a near-barrierless isomerization occurs.

Our images at both $m/z = 27$ and $m/z = 29$ show that the signal has two contributing sources: the dissociative ionization of the mass 57 parent radicals, as well as stable C_2H_5 products resulting from dissociation of some of the $CH_3C(O)CH_2$ radicals formed with enough internal energy to undergo subsequent dissociation to $C_2H_5 + CO$. The $m/z = 27$ signal is solely from dissociative ionization of these neutral C_2H_5 products, the appearance energy of which is below 10.5 eV.

While softer photoionization methods are often used to detect signal from radical and molecular species without the complication of dissociative ionization, the results herein definitively characterize the efficient dissociative ionization of $CH_3C(O)CH_2$ radicals to $m/z = 29$. Care should thus be taken in assigning $m/z = 29$ signal to the photoionization of ethyl radicals in measurements on multicomponent systems; $CH_3C(O)CH_2$ radicals also result in signal at this mass-to-charge ratio, even upon seemingly "soft" 10.5 eV photoionization.

Acknowledgements

This work was supported by the National Science Foundation under grant number CHE-0746050 (Butler). We gratefully acknowledge Daniel B. Straus, a current undergraduate researcher in our group, for developing the code used to model the detected speeds of the $C_2H_5^+$ products resulting from a two-step dissociation mechanism.

References

[1] G. Capozza, E. Segoloni, F. Leonori, G.G. Volpi, P. Casavecchia, Soft electron impact ionization in crossed molecular beam reactive scattering: the dynamics of the $O(^3P) + C_2H_2$ reaction, J. Chem. Phys. 120 (2004) 4557–4560.
[2] X. Yang, J. Lin, Y.T. Lee, D.A. Blank, A.G. Suits, A.M. Wodtke, Universal crossed molecular beams apparatus with synchrotron photoionization mass spectrometric product detection, Rev. Sci. Instrum. 68 (1997) 3317–3326.
[3] J.C. Robinson, N.E. Sveum, D.M. Neumark, Determination of absolute photoionization cross sections for vinyl and propargyl radicals, J. Chem. Phys. 119 (2003) 5311–5314.
[4] C.A. Taatjes, D.L. Osborn, T.A. Cool, K. Nakajima, Synchrotron photoionization measurements of combustion intermediates: the photoionization efficiency of HONO, Chem. Phys. Lett. 394 (2004) 19–24.
[5] V.A. Schubert, S.T. Pratt, Photodissociation of acetaldehyde and the absolute photoionization cross section of HCO^+, J. Phys. Chem. A 114 (2010) 11238–11243.
[6] B.W. Alligood, B.L. FitzPatrick, D.E. Szpunar, L.J. Butler, Chloroacetone photodissociation at 193 nm and the subsequent dynamics of the $CH_3C(O)CH_2$ radical –

an intermediate formed in the OH + allene reaction *en route to* CH_3 + ketene, J. Chem. Phys. 134 (2011) 054301.
[7] B.W. Alligood, D.B. Straus, C.C. Womack, L.J. Butler, manuscript in preparation (2011).
[8] M.J. Krisch, L.R. McCunn, K. Takematsu, L.J. Butler, F.R. Blase, J. Shu, Photodissociation of CH_3OCl to CH_3O + Cl at 248 nm, J. Phys. Chem. A 106 (2004) 1650–1656.
[9] M. Aschi, J.N. Harvey, C.A. Schalley, D. Schroder, H. Schwarz, Reappraisal of the spin-forbidden unimolecular decay of the methoxy cation, Chem. Commun. 5 (1998) 531–532.
[10] J.N. Harvey, M. Aschi, Spin-forbidden dehydrogenation of methoxy cation: a statistical view, Phys. Chem. Chem. Phys. 1 (1999) 5555–5563.
[11] K.-C. Lau, Y. Liu, L.J. Butler, Photodissociation of 1-bromo-2-butene 4-bromo-1-butene, and cyclopropylmethyl bromide at 234 nm studied using velocity map imaging, J. Chem. Phys. 125 (2006) 144312.
[12] B. Ruscic, J. Berkowitz, L.A. Curtiss, The ethyl radical: photoionization and theoretical studies, J. Chem. Phys. 91 (1989) 114–121.
[13] Y. Apeloig, M. Karni, B. Ciommer, G. Depke, G. Frenking, S. Meyn, J. Schmidt, H. Schwarz, $[CH_3COH]^{\bullet+}$, the central intermediate in the isomerization–dissociation reactions of ionized vinyl alcohol, J. Chem. Soc. Chem. Commun. (1983) 1497.
[14] N. Ohmichi, Y. Malinovich, J.P. Ziesel, C. Lifshitz, Time-dependent mass spectra and breakdown graphs. 12. Competitive dissociative isomerizations of the 2,4-hexadiyne cation, J. Phys. Chem. 93 (1989) 2491–2495.
[15] C. Lifshitz, N. Ohmichi, Time-dependent mass spectra and breakdown graphs. 13. Photoionization mass spectrometry of 1,5-hexadiyne, J. Phys. Chem. 93 (1989) 6329–6333.
[16] A.J.R. Heck, D.W. Chandler, Imaging techniques for the study of chemical reaction dynamics, Annu. Rev. Phys. Chem. 46 (1995) 335–372.
[17] A.T.J.B. Eppink, D.H. Parker, Velocity map imaging of ions and electrons using electrostatic lenses: application in photoelectron and photofragment ion imaging of molecular oxygen, Rev. Sci. Instrum. 68 (1997) 3477–3484.
[18] Y. Sato, Y. Matsumi, M. Kawasaki, K. Tsukiyama, R. Bersohn, Ion imaging of the photodissociation of OCS near 217 and 230 nm, J. Phys. Chem. 99 (1995) 16307–16314.
[19] Y. Liu, L.J. Butler, C–Cl bond fission dynamics and angular momentum recoupling in the 235 nm photodissociation of allyl chloride, J. Chem. Phys. 121 (2004) 11016–11022.
[20] B.J. Ratliff, X.N. Tang, L.J. Butler, D.E. Szpunar, K.-C. Lau, Determining the $CH_3SO_2 \rightarrow CH_3 + SO_2$ barrier from methylsulfonyl chloride photodissociation at 193 nm using velocity map imaging, J. Chem. Phys. 131 (2009) 044304.
[21] Y.T. Lee, J.D. McDonald, P.R. LeBreton, D.R. Herschbach, Molecular beam reactive scattering apparatus with electron bombardment detector, Rev. Sci. Instrum. 40 (1969) 1402–1408.
[22] N.R. Daly, Scintillation type mass spectrometer ion detector, Rev. Sci. Instrum. 31 (1960) 264–267.
[23] A.G. Baboul, L.A. Curtiss, P.C. Redfern, K. Raghavachari, Gaussian-3 theory using density functional geometries and zero-point energies, J. Chem. Phys. 110 (1999) 7650–7657.
[24] M.J. Frisch, G.W. Trucks, H.B. Schlegel, G.E. Scuseria, M.A. Robb, J.R. Cheeseman, J.A. Montgomery Jr., T. Vreven, K.N. Kudin, J.C. Burant, J.M. Millam, S.S. Iyengar, J. Tomasi, V. Barone, B. Mennucci, M. Cossi, G. Scalmani, N. Rega, G.A. Petersson, H. Nakatsuji, M. Hada, M. Ehara, K. Toyota, R. Fukuda, J. Hasegawa, M. Ishida, T. Nakajima, Y. Honda, O. Kitao, H. Nakai, M. Klene, X. Li, J.E. Knox, H.P. Hratchian, J.B. Cross, C. Adamo, J. Jaramillo, R. Gomperts, R.E. Stratmann, O. Yazyev, A.J. Austin, R. Cammi, C. Pomelli, J.W. Ochterski, P.Y. Ayala, K. Morokuma, G.A. Voth, P. Salvador, J.J. Dannenberg, V.G. Zakrzewski, S. Dapprich, A.D. Daniels, M.C. Strain, O. Farkas, D.K. Malick, A.D. Rabuck, K. Raghavachari, J.B. Foresman, J.V. Ortiz, Q. Cui, A.G. Baboul, S. Clifford, J. Cioslowski, B.B. Stefanov, G. Liu, A. Liashenko, P. Piskorz, I. Komaromi, R.L. Martin, D.J. Fox, T. Keith, M.A. Al-Laham, C.Y. Peng, A. Nanayakkara, M. Challacombe, P.M.W. Gill, B. Johnson, W. Chen, M.W. Wong, C. Gonzalez, J.A. Pople, GAUSSIAN03 Revision C. 02, Gaussian Inc., Pittsburgh, PA, 2003.
[25] B. FitzPatrick, Theoretical study of isomerization and dissociation transition states of C_3H_5O radical isomers: *ab initio* characterization of the critical points and statistical transition state theory modeling of the dynamics, J. Phys. Chem. A 115 (2011) 1701–1712.
[26] E.J. Hintsa, X. Zhao, Y.T. Lee, Photodissociation of 2-bromoethanol and 2-chloroethanol and 193 nm, J. Chem. Phys. 92 (1990) 2280–2286.